

# NUMERICAL SIMULATION STUDIES OF THE LBNL HEAVY-ION BEAM COMBINER EXPERIMENT

W.M. Fawley and P. Seidl, Lawrence Berkeley National Laboratory, Berkeley, CA 94720

I. Haber, Naval Research Laboratory, Washington, D.C. 20375

A. Friedman and D.P. Grote, Lawrence Livermore National Laboratory, Livermore, CA 94550

## Abstract

Transverse beam combining is a cost-saving option employed in many designs for heavy-ion inertial fusion energy<sup>1</sup> drivers. A major area of interest, both theoretically and experimentally, is the resultant transverse phase space dilution during the beam merging process. Currently, a prototype combining experiment is underway at LBNL and we have employed a variety of numerical descriptions to aid in both the initial design of the experiment as well as in the interpretation of the experimental data. These range from simple envelope codes to detailed 2- and 3-D PIC simulations. We compare the predictions of the different numerical models to each other and to experimental data at different longitudinal positions.

## 1 INTRODUCTION

In the heavy-ion approach to inertial fusion energy (IFE), transverse beam combining is an attractive, cost-savings option in many designs based on the induction linac approach. The basic reason for this is that in the low energy end of the accelerator near the injector, it is generally most cost-effective to employ electrostatic, quadrupole focusing. Due to electrical breakdown constraints, one is then forced to use subdivide the current into a large number of beamlets. As the beams accelerate to higher energies, eventually magnetic quadrupoles become more attractive for transverse focusing, in part because they more efficiently transport higher currents per beamlet. Hence, transverse beam-combining is seen as a useful (although not necessarily essential) transition from electrostatic to magnetostatic focusing.

Presently at LBNL, a prototype combining experiment employing the MBE-4 injector at 160 keV and four new Cs<sup>+</sup>, 5 mA sources is underway. The actual beam combining/merging region is composed of a number of electrostatic quadrupoles (labeled Q1-4) and a combined function elements (QD5) whose purpose is to first bring the four individual beamlets close together in a “Stonehenge” configuration, and then merge them into one large beam with (hopefully) minimal current loss and transverse phase space dilution. Details concerning the actual beamline layout of MBE-4 combiner experiment may be found in the accompanying paper Seidl *et al.*[1]. In support of the experiment, we have conducted a relatively extensive set of numerical simulations, employing a variety of codes ranging from simple envelope models to 2- and 3-D PIC sim-

ulations which include detailed modeling of the complex geometry of the focusing elements. Our basic concerns include obtaining good agreement with the measured beamlet properties both in the upstream (of QD5) transport region (where nonlinear effects are generally small) and the downstream region (where the merged beamlets have encountered strong nonlinear space charge fields and is undergoing mismatch oscillations). The remainder of this paper first discusses the simulation tools used in our study and then several comparisons between simulation and experimental data.

## 2 SIMULATION CODE DESCRIPTIONS

The **HIBEAM** 2D, electrostatic code was originally written by K. Hahn of LBNL and closely follows the structure of its forerunner, the venerable **SHIFT-XY**[2]. **HIBEAM** has recently been ported to Fortran90 which has aided considerably in its maintainability and extendibility. The field solver employs an FFT together with a capacity matrix for inclusion of conducting electrodes (and image charges thereon). At present, the code does not include a fringe field model.

Our most comprehensive simulation tool for modeling the combiner experiment is the 3D, electrostatic PIC code **WARP3D**[3]. Via an FFT or SOR field solver, the code models the full 3D fields of both the heavy-ion beam and of conducting electrodes, including fringe and image charge components. Unfortunately, we were unable to complete the necessary coding in **WARP3D** to model the QD5 “squirrel cage” combined function element. Consequently, the **WARP3D** simulations stop just upstream at the M2 diagnostic. For computational efficiency, the simulations model the time-steady transport of the longitudinal beam center. This is done by continuously injecting beam at the upstream entry plane and, once a time-steady state is evident throughout the simulation grid, stopping the simulation and diagnosing beam properties as a function of  $z$ .

## 3 BEAM BEHAVIOR FROM THE SOURCE TO THE M2 DIAGNOSTIC PLANE

We began the numerical simulations at an entry plane just beyond the cathode plate which terminates the diode. These simulations model the “unapertured” beamlets with initial currents of 4.8 mA and normalized “edge” emittances of  $2.0 \times 10^{-8}$  m-rad. Since there was no phase space diagnostics at the entry plane, it was necessary to infer the initial beam conditions by using experimental data for

<sup>1</sup>see the U.S. HIF WWW site <http://fusion.lbl.gov/>

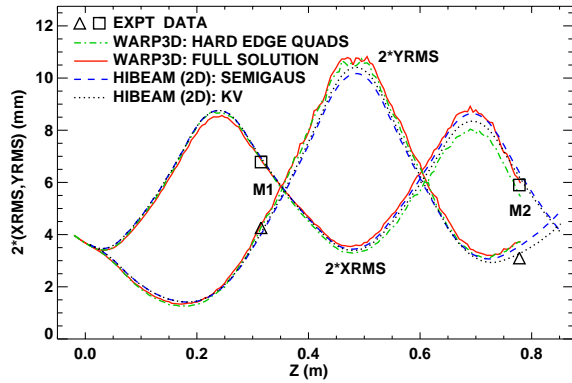


Figure 1: Predicted  $x$  and  $y$  beam envelope extents plotted versus  $z$  from both HIBEAM and WARP3D simulation code results. The open triangles and squares refer to experimental data taken at the M1 and M2 diagnostic planes.

( $a, b, a', b'$ ) at the M1 diagnostic location 0.315 m downstream and then integrating the envelope equation backwards. Figure 1 displays the HIBEAM and WARP3D predictions for the beamlet envelope (defined to be twice the RMS radius) in each plane together with experimental measurements at M1 and M2. Two sets of WARP3D results are shown: one corresponding to a full field solution and a second set (“HARD EDGE QUADS”) in which the voltages on the quadrupole electrodes were set exactly to zero and an external, linear focusing field was applied at those  $z$ -locations corresponding to the quadrupole rods. This field solution thus ignores higher order multipoles and fringe field terms but does include the effects of image charges. The two HIBEAM runs differ only in the initial phase space distributions, one employing a semi-Gaussian and the other a K-V distribution. One sees that, not surprisingly, there is good agreement between experiment and simulation for beam envelope sizes at M1 and fair agreement at the M2 diagnostic location.

We believe that the discrepancies between the experimental data and simulation results at M2 arise for a number of reasons. First, the large excursions (see Fig. 1) in the envelope radii in both planes (especially the tight focus of  $\approx 1.5$  mm at  $z=0.18$  m near Q2) cause the beam behavior downstream of Q2 to be quite sensitive to the transport system parameters. For example a change of only a few percent in the quadrupole gradients of one of the lenses can result in a substantial movement of the longitudinal position of a downstream beam waist which occurs quite close to the M2 diagnostic plane. Such movement can significantly modify the predicted beam divergence/convergence angles  $a', b'$  at M2. Similarly, small differences between the numerical code representation and the actual physical structures, such as might arise from numerical algorithm inaccuracies or alignment errors, can also be magnified by this effect. Second, an additional source of uncertainty results from the use of the backward integration of envelope equation from M1 to infer beam parameters at the entry

plane. If the beam phase space deviates in any significant fashion from the presumed K-V distribution of the envelope solution, this produces an additional inconsistency between the assumed entry condition and the actual experiment. Since the HIBEAM K-V simulation shows the best agreement at M2 for beam envelope size, we suspect that a more direct measurement of beam phase space properties near the entrance plane would produce much better agreement between the semi-Gaussian runs of both WARP and HIBEAM.

One of the more gratifying comparisons to come out so far between experiment and simulation is the actual phase space shape at the M2 diagnostic location. In the  $y - y'$  projection (where the beamlet is just beyond a waist and diverging), both HIBEAM (Fig. 2) and WARP3D (not shown) predict a pronounced “S”-ing. This is also seen clearly in the experimental measurements (Fig. 3). Surprisingly, this shape is *not* due to focusing nonlinearities but rather to the strong compression of the initially semi-Gaussian phase space distribution near Q2. If a K-V initial distribution is chosen for the simulation, no such “S” develops. It appears that the semi-Gaussian’s thermal spread in velocity space is rotated into a “halo” in configuration space at the beam waist, which is accompanied by a strong nonlinear space charge force in the outer portions of the beam. This nonlinearity then results in the outermost particles having a smaller tune depression and thus rotating more rapidly in phase space with  $z$ . The commonality of 2- and 3-D simulation results has been extremely useful in delineating the physics underlying the phase space distortion.

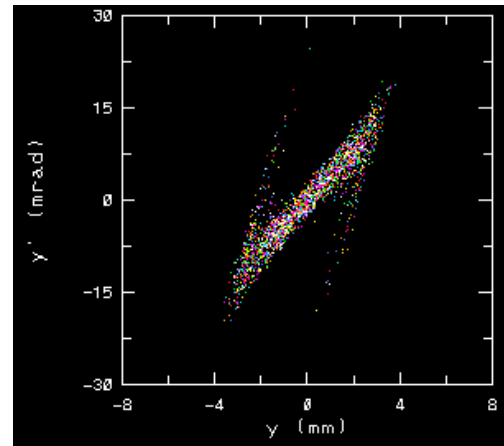


Figure 2: HIBEAM-predicted  $y - y'$  phase space at the M2 diagnostic location. This run was initialized with a semi-Gaussian phase space distribution.

#### 4 BEAM BEHAVIOR IN THE QD5 “SQUIRREL CAGE”

The last focusing element before the beamlet merge point is the combined function (dipole/quadrupole) electrostatic element QD5 commonly referred to as the “squirrel cage”. Approximately 70 separate, cantilevered tungsten rods sur-

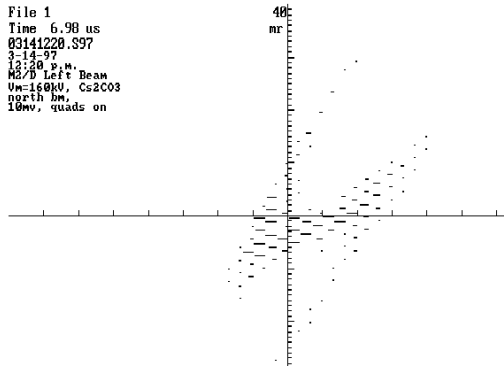


Figure 3: Experimental phase space data at the M2 diagnostic location for the left beamlet. The length of the horizontal bars indicate the signal amplitude. The major tick marks on the abscissa correspond to 1 mm intervals.

round four separate openings arranged in a tapered (with  $z$ ) “Stonehenge” geometry for the individual beamlets. The beamlets enter the cage at a six degree angle relative to the downstream central axis with a converging focus in the transverse plane parallel to their offset. The individual voltages on the tungsten rods are designed to remove both the six degree angle (via the dipole component) and the convergence (via the quadrupole component) by the exit point from the cage.

Utilizing a 3D capacity matrix in order to take into account the effects of the taper, fringe fields, and the discrete azimuthal nature of the rods (but not image charge forces), we performed detailed calculations[4] during the design stage to determine an optimum set of individual voltages for the squirrel cage rods. In Fig. 4 we plot the predicted beam offsets versus  $z$  from both the full 3D calculation (which uses the values of the  $z$ -varying line charges on the discrete tungsten rods) and the HIBEAM code results (whose 2D solution includes the local effect of the taper but not fringe fields). In this figure, the cage extends longitudinally from -40 to +40 mm. In order to remove (empirically) the full six degree offset by cage exit, it was necessary in the HIBEAM calculation to increase the cage voltages a uniform 14% from their nominal values. This correction was *not* necessary for the 3D solution - examination of  $y'(z)$  for the top cage and  $x'(z)$  for the side cage respectively shows that both the upstream and downstream fringe fields remove approximately 6 mrad from the input 105 mrad angle which we believe is the major difference between the 2- and 3-D calculations. Experimentally, it appears (as of May 1997) that the nominal cage voltages may be slightly (of order a few percent) *too high*. If so, this may be related to details of the exact geometry that the wire leads in the individual rods follow of the MACOR plate supporting the cage assembly (A. Faltens, private communication). Any “energy effect” (which is not modeled in HIBEAM) would be in the opposite direction because each beam accelerates a couple percent as it enters the cage.

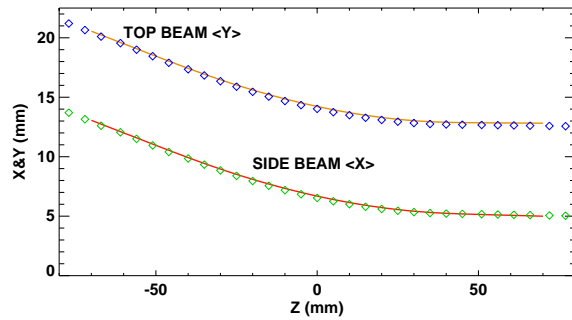


Figure 4: Top and side beam offsets in the squirrel cage (relative to the downstream central axis). The solid lines are predictions using the “exact” 3D capacity matrix solution whereas the open triangles are HIBEAM simulation results.

## 5 MERGED BEAM BEHAVIOR BEYOND THE SQUIRREL CAGE

With the cage exit at 0.96 m downstream of the entry plane, the first diagnostic location beyond the merge point is M4 at 1.33 m, by which point the beamlets have passed the Q6 and Q7 quadrupoles. Although the predicted nonlinear curvature for each beamlet is small (see Fig. 3 of Ref.[1]) one notices that divergence angles of the outboard beamlets visibly differ from that of inboard beamlets. This undesirable feature arose from upstream lattice modifications necessary both because of the larger current of the unapertured beamlets and an accompanying increase in their convergence angles at the diode exit relative to the original the original design values. After eventual downstream phase mixing, this produces a greater final emittance than would be true otherwise.

Preliminary M4 experimental data is in good agreement with both the beam sizes and the overall convergence/divergence angles but is insufficiently detailed to make fine comparisons on the sub-10-mrad scale.

## 6 ACKNOWLEDGEMENTS

This work was supported by the U.S. Department of Energy under Contracts No. DE-AC03-76SF00098 (LBNL), DE-AI02-94ER54232 (NRL), and W-7405-ENG-48 (LLNL), and used computational resources of the DOE NERSC.

## 7 REFERENCES

- [1] P.A. Seidl *et al.*, “A Scaled Beam-Combining Experiment for Heavy Ion Inertial Fusion”, these proceedings, Paper 8V46.
- [2] I. Haber, in *High Current, High Brightness, High Duty Factor Ion Injectors*, **AIP Conf. Proc.** **139**, Ed. G.H. Gillespie, (Amer. Inst. Physics, New York, 1986), p. 107 (1986).
- [3] A. Friedman, D.P. Grote, D.A. Callahan, A.B. Langdon, and I. Haber, *Part. Accel.*, **37-38**, 131 (1992).
- [4] W.M. Fawley: “Life on the Edge: Squirrel-Cage Fringe Fields and Their Effects in the MBE-4 Combiner Experiment”, LBNL report *LBL-38399* (1996).